Journal of Biological Physics 31: 417–432, 2005.
DOI: 10.1007/s10867-005-0173-0

A Spectroscopic Study of Structural Heterogeneity and Carbon Monoxide Binding in Neuroglobin

KARIN NIENHAUS[1] and G. ULRICH NIENHAUS[1,2,*]
[1]*Department of Biophysics, University of Ulm, Albert-Einstein-Allee 11, 89081 Ulm, Germany;*
[2]*Department of Physics, University of Illinois at Urbana-Champaign, 1110 West Green Street, Urbana, IL 61801, U.S.A.*
*(*Author for correspondence, e-mail: uli@uiuc.edu)*

Abstract. Neuroglobin (Ngb) is a small globular protein that binds diatomic ligands like oxygen, carbon monoxide (CO) and nitric oxide at a heme prosthetic group. We have performed FTIR spectroscopy in the infrared stretching bands of CO and flash photolysis with monitoring in the electronic heme absorption bands to investigate structural heterogeneity at the active site of Ngb and its effects on CO binding and migration at cryogenic temperatures. Four CO stretching bands were identified; they correspond to discrete conformations that differ in structural details and CO binding properties. Based on a comparison of bound-state and photoproduct IR spectra of the wild-type protein, Ngb distal pocket mutants and myoglobin, we have provided structural interpretations of the conformations associated with the different CO bands. We have also studied ligand migration to the primary docking site, B. Rebinding from this site is governed by very low enthalpy barriers (∼1 kJ/mol), indicating an extremely reactive heme iron. Moreover, we have observed ligand migration to a secondary docking site, C, from which CO rebinding involves higher enthalpy barriers.

Key words: FTIR spectroscopy, ligand binding, neuroglobin, temperature derivative spectroscopy

1. Introduction

Proteins are biological macromolecules that perform a wide variety of tasks in living organisms [1]. Their three-dimensional structures are designed and fine-tuned to carry out specific functions. Due to comparatively weak forces stabilizing their native structure, proteins are fluctuating entities that can assume many slightly different structures called conformational substates, which can be represented as local minima on a rough energy surface [2, 3]. In 1985, Frauenfelder and coworkers proposed that conformational substates are arranged in a hierarchical fashion, involving several levels or tiers of substates [4, 5]. This concept was originally developed on the basis of detailed experimental investigations, using sperm whale myoglobin (Mb) as a model system. Over the years, further evidence for a hierarchical energy landscape has been accumulated both by theoretical [6–8] and experimental studies [9–11] on a variety of proteins.

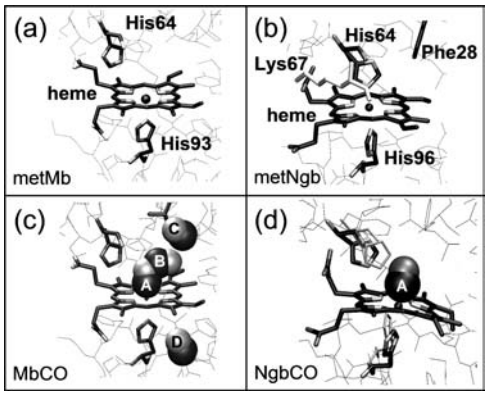

Figure 1. Structures of the active sites of sperm whale Mb and murine Ngb. The heme plane and selected amino acids are highlighted. (a) Ferric Mb; (b) Ferric Ngb. K67 (in light gray) is located in the foreground. (c) MbCO: The CO ligand is included at the binding site A, at intermediate site B (pdb 1ABS, [59]) and in the Xe4 (site C) and Xe1 (site D) cavities (pdb codes 1DO3 and 1DO4, [23]). (d) NgbCO (pdb code 1W92, [32]). The positions of H64 and H96 in the ferric Ngb structure are included in gray.

In myoglobin (Mb), small diatomic ligands such as CO, O_2 or NO can bind at a heme prosthetic group (Figures 1a and c). Different orientations of the distal histidine H64 within the distal heme pocket give rise to three infrared (IR) stretching bands of the heme-bound CO that have been associated with three taxonomic substates [12–16]. The different IR bands originate from electrostatic interactions (Stark effects) of the CO dipole with the electric field created by its local environment [13, 17].

In sperm whale MbCO, the infrared absorbance bands of heme-bound CO are denoted as A_0, A_1 and A_3 [18–21]. After photodissociation at cryogenic temperatures, the CO ligands are trapped within the Mb protein matrix and can reside in different locations, namely, the primary docking site, B, and the secondary docking sites, C and D (Figure 1c) [19, 20, 22, 23]. In these docking sites, the trapped CO molecules display stretching bands specific of the individual photoproduct site. Typically, two IR bands are observed for each intermediate site because the CO molecule can adopt two opposite orientations within the cavity, which yields a doublet of IR bands in the presence of a local electric field [17]. The primary docking site B is located on top of the heme plane, and it mediates ligand binding [24, 25]. Secondary sites C and D correspond to internal protein cavities Xe4 and Xe1 [26]. They provide alternate locations for dissociated ligands, so that the probability of geminate recombination is reduced during the time that the ligands have to wait for large-scale protein motions to open transient entry and exit pathways.

Neuroglobin (Ngb) is a small heme protein, discovered recently in the human brain [27], with an as yet unknown physiological function. Its low expression level and moderate oxygen affinity (half saturation pressure $P_{50} \approx 2.0$ torr [27]) suggests

a function different from simple oxygen storage and transport [28]. A variety of studies indicate that Ngb is a sensor protein that responds to oxidative stress [28–31]. This suggestion is also supported by our findings that Ngb undergoes a significant structural change upon ligand binding [32].

Analogous to MbCO, wild-type (wt) NgbCO also shows multiple infrared bands of heme-bound CO [32, 33] corresponding to different active site conformations that might be functionally relevant. The three-dimensional structures of human [34] and mouse [35] Ngb show the typical 3-over-3-α-helical sandwich fold surrounding the heme prosthetic group. The oxidized (ferric, Fe^{3+}) heme iron is coordinated by both the distal (H64) and proximal (H96) histidines (Figure 1b). Hexacoordination is retained in the reduced (ferrous, Fe^{2+}) form [36–39]. Consequently, the endogenous H64 ligand has to be removed from the sixth coordination site to enable exogenous ligand binding (Figure 1d). Quite unexpectedly, it is not the H64 imidazole side chain that reorients to make room for the exogenous ligand. Instead, the heme plane slides deeper into the protein to provide access to the sixth coordination site [32].

Here we present a detailed investigation of structural heterogeneity, ligand binding and migration in NgbCO, using flash photolysis with monitoring in the visible and Fourier transform infrared (FTIR) spectroscopy in the CO stretching bands. We have also prepared a number of mutants to examine the influence of the key residues histidine H64 and lysine K67 on the neuroglobin structure, spectroscopy and ligand binding properties. Comparisons of wild-type (wt) Ngb with these mutants and MbCO enabled us to partially assign the different infrared bands to specific conformations. Implications of structural heterogeneity on ligand migration and binding will be discussed, also with respect to the heme-sliding mechanism that became apparent in the X-ray structure of NgbCO [32].

2. Materials and Methods

2.1. Sample Preparation

Lyophilized protein was dissolved in 75%/25% (v/v) glycerol/buffer to a final concentration of $\sim$10 mM (samples for infrared spectroscopy) and 10 μM (samples for flash photolysis with monitoring in the visible range). To prepare the CO derivative, solutions were equilibrated with 1 bar of CO and reduced by adding a twofold molar excess of sodium dithionite.

2.2. Flash Photolysis

The sample was sealed in a $10 \times 10 \times 2.5\,mm^3$ polymethylmethacrylate (PMMA) cuvette and attached to the cold finger of a closed-cycle helium refrigerator. Experiments were carried out with a home-built flash photolysis apparatus, using a 6-ns (full width at half maximum) pulse from a frequency-doubled Nd:YAG laser (model Surelite, Continuum, Santa Clara, CA) for photodissociation. Ligand

binding was monitored with light from a tungsten source which was passed through a monochromator set at 436 nm. A photomultiplier tube (model R5600U, Hamamatsu Corp., Middlesex, NJ) measured the intensities. These data were recorded with a digital storage oscilloscope from 10 ns to 50 μs (model TDS 520, Tektronix, Wilsonville, OR) and a home-built logarithmic time-base digitizer (Wondertoy II) from 2 μs to 100 s.

2.3. Fourier Transform Infrared Spectroscopy (FTIR)

The sample solution was centrifuged prior to loading into the sample cell to remove any undissolved protein. A few microliters of the protein solution were sandwiched between two CaF_2 windows (diameter 25.4 mm) separated by a 75 μm mylar washer. The sandwich was placed in a copper block and mounted on the cold finger of a closed-cycle refrigerator (model SRDK-205AW, Sumitomo, Tokyo, Japan). The temperature was measured with a silicon diode (model DT 470, Lakeshore Cryotronics, Westerville, OH) and adjusted in the range 3–200 K by a digital temperature controller (model 330, Lakeshore Cryotronics, Westerville, OH). Transmission spectra were collected in the mid-IR region (1800–2400 cm^{-1}) with a resolution of 2 cm^{-1} with a Fourier transform infrared (FTIR) spectrometer (IFS 66v/S, Bruker, Karlsruhe, Germany). To measure the overall stretching bands of heme-bound CO, we collected transmission spectra of NgbCO and metNgb (oxidized Ngb that does not bind CO) as a reference. Absorbance difference spectra were calculated as $\Delta A = -\log(I_{\mathrm{metNgb}}/I_{\mathrm{NgbCO}})$. To measure photolysis difference spectra, NgbCO samples were photodissociated by using a continuous-wave, frequency-doubled Nd:YAG laser (model Forte, 530-300, Laser Quantum, Manchester, UK) with 300 mW output at 532 nm. Transmission spectra were collected before and after illumination, from which absorbance difference spectra were calculated as $\Delta A = -\log(I_{\mathrm{light}}/I_{\mathrm{dark}})$, revealing the light-induced absorbance changes within each sample. Two different illumination protocols were employed. In a first experiment, the samples were cooled to 3 K in the dark. Subsequently, they were illuminated for 1 s, which corresponds to $\sim$20 photon absorption events per heme molecule. With this procedure, CO migration to remote locations after photolysis will be minimal. For example, in wild-type MbCO, ligands will only migrate to the primary docking site B after photolysis at 3 K, but not to C or D (Figure 1c). Additional intermediate sites, which may only be accessible after the ligands surmount higher activation barriers, can be populated by cooling the samples from higher temperature, e.g. from 140 to 3 K, under constant illumination, as we have shown for wild-type MbCO and various mutants [22, 40, 41].

2.4. Temperature Derivative Spectroscopy (TDS)

This experimental protocol allows one to study thermally activated rate processes governed by enthalpy barrier distributions [22, 42, 43]. Initially, a non-equilibrium

intermediate state is created by photolysis. The subsequent temperature derivative spectroscopy TDS measurement records the dynamics in the sample in the dark by means of a spectroscopic marker while the temperature is increased linearly in time (5 mK/s in the experiments presented here). Here we use the CO stretching vibration as a marker, taking one FTIR spectrum every kelvin while ramping the temperature. The absorbance change, $\Delta A(\nu, T)$, that occurs from one spectrum to the next is calculated by taking the difference between successive spectra; it approximates the derivative. The absorbance change may arise from ligand rebinding to the heme iron, ligand migration to alternative locations in the interior of the protein, ligand dynamics in a particular site and conformational changes of the protein [17, 19, 20]. The temperature ramp protocol ensures that ligand rebinding occurs sequentially with respect to the height of the activation enthalpy barriers that must be surmounted by the CO ligand to form a covalent bond to the heme iron. At the lowest temperatures, only proteins with small enthalpy barriers recombine. With increasing temperature, more thermal energy becomes available so that successively higher barriers can be surmounted. For simple two-state processes governed by the Arrhenius law, the temperature axis can be converted into an enthalpy axis [42]. We present TDS data using logarithmically spaced contour plots, with solid lines indicating an absorbance increase and dashed lines a decrease.

3. Results and Discussion

3.1. Flash Photolysis

After exposure of an NgbCO sample to an intense nanosecond laser flash at cryogenic temperatures, CO ligands are photodissociated from the heme iron and trapped within the protein matrix. The subsequent recombination process can be monitored through the absorbance change in the Soret band at 432 nm as a function of time and temperature. To a good approximation, the observed absorbance difference, $\Delta A(t)$, can be taken as proportional to the survival probability $N_B(t)$ of CO ligands in the photodissociated state. The kinetics of NgbCO, shown in Figure 2 for temperatures between 20 and 120 K, are nonexponential and can be fitted with a two-state model with a static enthalpy barrier distribution $g(H_{BA})$ between a heme-bound state A and a photoproduct state B (Figure 2, lines). The survival probability $N_B(t)$ in the deligated state B is given by

$$N_B(t) = \int g(H_{BA}) \exp[-k_{BA}(T)t] dH_{BA}, \tag{1}$$

assuming that the temperature dependence of the rate coefficient k_{BA} is governed by the Arrhenius law,

$$k_{BA}(T) = A_{BA} \frac{T}{T_0} \exp\left(-\frac{H_{BA}}{RT}\right), \tag{2}$$

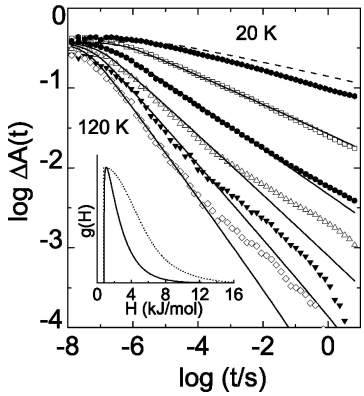

Figure 2. Flash photolysis kinetics of wt NgbCO in 75% glycerol, 25% 0.4 M potassium phosphate buffer (v/v), pH 8, measured at 436 nm for temperatures between 20 and 120 K. The solid lines represent the kinetics as calculated from a global fit with Eqs. (1–3). Inset: Enthalpy barrier distributions obtained from flash photolysis (solid line) and TDS experiments (dotted line).

with pre-exponential A, reference temperature T_0 set to 100 K, temperature T and universal gas constant R. For the fit in Figure 2, the enthalpy barrier distribution $g(H_{BA})$ was modeled as a Γ-distribution [44, 45],

$$\Gamma(H_{BA}) \propto (H_{BA} - H_{\min})^{\alpha(H_{\text{peak}} - H_{\min})} \exp[-\alpha(H_{BA} - H_{\min})]. \quad (3)$$

The global nonlinear least-squares fit of this model to the data from 40 to 120 K (Figure 2, lines) shows that the Γ-distribution peaks at 1.1 ± 0.2 kJ/mol (inset Figure 2). The pre-exponential A was determined as $10^{7.8\pm0.5}\,\text{s}^{-1}$ [33], $\alpha = 0.58 \pm 0.05$ mol/kJ, and $H_{\min} = 0.8 \pm 0.1$ kJ/mol. The fit was limited to the temperature interval between 40 and 120 K because quantum-mechanical tunneling will markedly affect the recombination kinetics at the very lowest temperatures [45, 46]. Indeed, recombination is faster as the prediction from the Arrhenius model at 20 K (dotted line in Figure 2).

A pronounced deviation from the simple two-state model is apparent at longer times for a minor fraction of the total population (Figure 2). Starting at 60 K, a second, slower process becomes apparent. This observation can be explained by assuming that a small fraction of molecules ($<1\%$) escapes to another intermediate site C with higher activation enthalpy barriers against recombination. This interpretation will be substantiated by the TDS experiments discussed below.

Ligand rebinding in NgbCO is extremely fast, as reflected by its barrier distribution peaking at 1.1 kJ/mol. In contrast, MbCO rebinds much more slowly, and the fit of the kinetics with a Γ-distribution yields a peak at $\sim$10 kJ/mol [47–49]. Given that both proteins have the identical heme group, this comparison raises the question about the structural determinants that govern the rebinding barrier at the heme iron. Here, one can distinguish between two contributions, (1) steric hindrance by

nearby residues that prevent ligand access to the binding site, and (2) reactivity of the heme iron itself, which may be affected by the way the heme is embedded in the globin moiety. Especially, the iron-out-of-plane distance has been identified as an important structural parameter governing heme iron reactivity [50]. In MbCO, H64 plays a key role in regard to steric hindrance. Removal of this side chain in H64L MbCO leads to an enthalpy distribution peaking at 6.5 kJ/mol (unpublished results). This value is still much larger than the one in NgbCO, which suggests that H64 in NgbCO does not exert much steric hindrance towards CO rebinding, and furthermore, that the low barriers are caused by a highly reactive heme iron.

3.2. Structural Heterogeneity in the CO-Bound State

The infrared stretching bands of heme-bound CO (Figure 3) are known to be excellent reporters of structural heterogeneity in globins due to their exquisite sensitivity

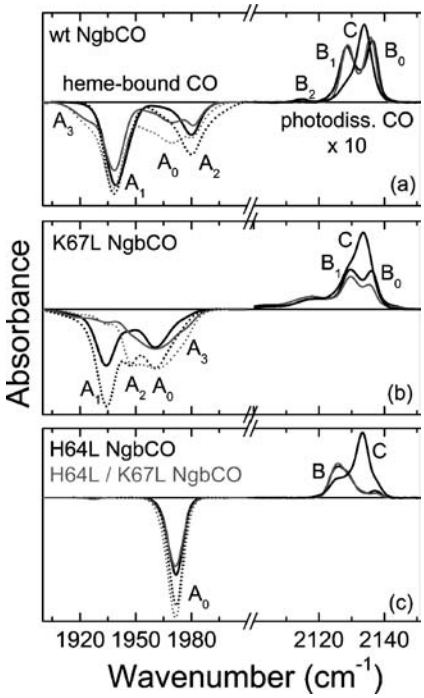

Figure 3. FTIR difference spectra of NgbCO and mutants. Photolysis difference spectra (solid lines) were calculated from transmission spectra collected before and after 1-s illumination at 3 K in the spectral regions of heme-bound and photolyzed CO. FTIR absorbance spectra (dotted lines) calculated from NgbCO transmission spectra before photolysis and metNgb transmission spectra show the overall heme-bound CO. (a) wt NgbCO, pH 7.3 (black) and pH 5.3 (light gray). (b) K67L NgbCO, pH 7.5 (black) and pH 5.5 (light gray). (c) H64L NgbCO (pH 7.3, black) and H64L-K67L (pH 7.4, light gray). The photoproduct spectra after extended illumination (slow-cooling from 140 to 3 K) are included in dark gray.

to local electric fields that are created by amino acid residues surrounding the active site [17, 51, 52]. For wt NgbCO at pH 7.3, essentially two stretching bands of heme-bound CO are observed (Figure 3a, black lines), corresponding to two discrete conformations, A_1 (1938 cm^{-1}) and A_2 (1980 cm^{-1}). Comparison of the overall spectra (dotted lines) and the photolysis difference spectra (solid lines) shows that a substantial fraction of A_2 rebinds in the 200 s after photodissociation during which the FTIR spectrum is acquired. At pH 5.3 (grey lines), two additional conformations can be clearly distinguished, A_0 (1968 cm^{-1}) and A_3 (1923 cm^{-1}). The NgbCO mutant K67L also shows four CO stretching bands (Figure 3b), which we assign to conformations A_0 (1960 cm^{-1}), A_1 (1933 cm^{-1}), A_2 (1947 cm^{-1}) and A_3 (1975 cm^{-1}). However, only the CO ligands in protein molecules of conformations A_3 and A_0 can be kept photodissociated longer than the time it takes to collect a spectrum (200 s), as can be seen by comparing the overall and photolysis difference spectra (Figure 3b). Replacement of the distal histidine by leucine in H64L NgbCO results in an active site with only a single conformation, as indicated by the CO stretching band A_0 at 1972 cm^{-1} (Figure 3c). The identical band is also observed in double mutant H64L-K67L. The peak frequencies and line widths of NgbCO and its distal pocket mutants are compiled together with data on wt MbCO and H64L MbCO in Table I.

Comparison of the CO stretching bands of NgbCO and MbCO affords some insights into the structural properties of the conformations observed for NgbCO. For both proteins, replacement of H64 by leucine results in a single conformation, characterized by a band at 1960–1970 cm^{-1} (Table I). This observation suggests that H64 is by and large responsible for the active site heterogeneity sensed by the CO molecule. Wild type MbCO has two major A substates at high pH, associated with the dominant A_1 (1945 cm^{-1}) and the weaker A_3 (1933 cm^{-1}) bands [16]. The structures associated with these states are characterized by a neutral H64 imidazole side chain residing in the distal pocket close to the heme iron [14, 53], placing a

Table I. Peak frequencies and full widths at half maximum, as determined from Gaussian fits, of CO stretching bands in NgbCO and MbCO below 20 K.

		Band positions (widths) [cm^{-1}]							
Protein	pH	A_0	A_1	A_2	A_3	B_0	B_1	B_2	C
wt NgbCO	5.3	1969(17)	1939(12)	1982(10)	1925(17)	2136(5)	2129(6)	2115(6)	2134(6)
	7.3		1939(14)	1980(11)		2136(5)	2129(6)		2134(6)
K67L NgbCO	5.5	1960(23)	1933(11)	1946(9)	1975(15)	2136(6)	2130(7)		2134(7)
	7.5	1960(21)	1934(13)	1947(8)		2136(6)	2130(7)		2134(7)
H64L NgbCO	7.3	1972(9)				2137(6)	2126(9)[a]		2133(6)
H64L-K67L NgbCO	7.4	1971(9)				2137(6)	2126(9)[a]		2133(6)
wt MbCO	7.0	1966(9)	1945(8)		1928(20)	2149(7)	2131(7)	2118(5)	2132(7)
H64L MbCO	7.3	1965(5)				2126(5)			2132(6)

[a]This band most likely consists of two bands.

positive partial charge from the $N_{\varepsilon 2}$ hydrogen near the CO, thereby lowering the frequency from 1966 cm^{-1}. Apparently, two stable positions of H64, with markedly different interactions with the CO, cause the two bands A_1 and A_3 in MbCO. It has been noticed that MbCO mutants with bulky amino acids such as phenylalanine or tyrosine at position 10 in the B helix have A_3 as the dominant substate [13, 40]. Ngb has a phenylalanine F28 at this position, and consequently, its dominant band, which we denote A_1, is actually related to the A_3 band in MbCO. Its frequency at 1939 cm^{-1} is higher than the one of A_3 in MbCO. However, this may be due to the presence of a positively charged lysine K67 that forms a salt bridge with one of the heme propionates. The electron-withdrawing effect on the heme macrocycle will lower the backbonding capability of the heme iron, which should result in a higher frequency of the CO stretching band [16, 54, 55]. Indeed, K67L NgbCO, which cannot form a hydrogen bond, has its dominant band A_1 at 1933 cm^{-1}, which is essentially the frequency of A_3 in wt MbCO. A similar, or possibly even larger shift is observed for the A_0 substate due to the K67L mutation.

The A_0 band in MbCO is located at $\sim$1967 cm^{-1}, at a similar frequency of the H64L mutant, which suggests that the H64 side chain does not interact with the CO in this conformation. It appears at low pH, when the H64 imidazole protonates and swings out of the heme pocket [16, 53]. Wild type NgbCO also develops an A_0-type band at low pH (Figure 3a). The simultaneous gain of A_0 and loss of A_1 with decreasing pH suggests that, in analogy to MbCO, the H64 imidazole side chain gets protonated and swings out of the heme pocket [16], as recently also suggested by Couture *et al.* [56]. In fact, the pK of this protonation is 4.4 and thus essentially identical to the value for MbCO [36]. In aqueous solution, a pK of $\sim$6.0 is expected for the imidazole side chain of histidine. The marked deviation from this value reflects the fact that the imidazole resides in a hydrophobic distal pocket, so that protonation becomes much less probable due to the lack of access for water.

While this provides a reliable correlation of the A_0 and A_1 substates of NgbCO to A_0 and A_3 in MbCO, an assignment of the other two substates of NgbCO is more ambiguous. The A_2 band of wt NgbCO appears at a comparatively high frequency of 1980 cm^{-1}. IR bands at wavenumbers well above 1965 cm^{-1} have been reported for Mb mutants that place negative charges close to the ligand oxygen, for instance, H64V/V68T MbCO at 1984 cm^{-1} [13]. The high-frequency A_2 band of wt NgbCO may arise from a strong interaction of the π-electron system of phenylalanine F28 with the bound ligand (Figure 1b). It could also represent a conformation where the $N_{\delta 1}$ nitrogen of H64 is protonated so that the non-bonding electron pair of the $N_{\varepsilon 2}$ nitrogen resides in close vicinity of the heme-bound ligand. Free histidine in solution is a mixture of both tautomers, with a 4:1 preference for the protonated $N_{\varepsilon 2}$ [57]. While the neutral H64 side chain in MbCO always seems to reside in the heme pocket with a protonated $N_{\varepsilon 2}$ atom, we note that, in Ngb, only the $N_{\delta 1}$ tautomer can form the hexacoordinate ferrous species after dissociation of the exogenous ligand [36]. Therefore, this conformation has relevance for the function of Ngb. In wt NgbCO, the population in A_2 decreases with pH, which indicates that H64 is

neutral in this conformation. In K67L NgbCO, however, the band denoted by A_3 (1975 cm^{-1}) has a similar high frequency. Yet, this band increases together with A_0 upon lowering the pH, which implies that the H64 side chain is protonated in this case. Moreover, the broad A_0 and A_3 bands in the K67L mutant suggest that water may enter the distal pocket at low pH. In the wild-type protein, the long side chain of K67 forms a salt bridge to a heme propionate and thus protects the active site from the solvent (Figure 1). The pK of H64 in K67L NgbCO is 5.6 instead of 4.4 for the wt protein [36], and thus closer to the normal pK of histidine. This indeed suggests a more solvent-accessible distal pocket in K67L NgbCO. The fourth A substate band of K67L NgbCO is difficult to discern from its neighboring bands. It is, however, remarkable that ligands in the A_2 conformation (1947 cm^{-1}) cannot be trapped long enough at intermediate docking sites to be detected in the photolysis difference spectra (Figure 3b).

Low-frequency bands of heme-bound CO are observed whenever a residue with a strong positive partial charge is positioned close to the oxygen atom of the CO molecule. For instance, the interaction of an amino group of an asparagine side chain shifts the CO stretching frequency to 1916 cm^{-1} in V68N MbCO [13]. In the Hb from *Mycobacterium tuberculosis* [58], the low CO stretching frequency is caused by a tyrosine in helix B position 10 that stabilizes the ligand by a hydrogen bond. In wt NgbCO, the band denoted as A_3 (1925 cm^{-1}) is only present at low pH. Therefore, it is associated with a protonated H64 side chain. It is possible that a fraction of protonated imidazole side chains remains in the distal heme pocket, thus providing the positive charge responsible for the down-shift of the CO stretching band. Another residue in the vicinity of the heme iron that is capable of providing a positive partial charge is K67 (Figure 1). Clear structural evidence can only be provided by an x-ray structure of the low-pH form of NgbCO.

Finally, we note that the widths of the individual CO stretching bands in NgbCO and its variants are larger than the ones of their counterparts in MbCO [12], especially for the bands that appear at low pH (Table I). This observation indicates that the Ngb heme pocket features a pronounced statistical heterogeneity within each taxonomic substate.

3.3. Structural Heterogeneity at Photoproduct Sites B and C

After 1-s illumination at 3 K, two pronounced photoproduct bands, B_1 and B_0, are seen for wt and K67L NgbCO (Figure 3). B_2 at 2115 cm^{-1} is only visible at high pH. In analogy to MbCO [25, 52], we propose that the two main bands arise from Stark splitting of the CO bands in the local electric field at the primary docking site B, where the ligands can reside in opposite orientations (Figure 1c). In K67L NgbCO, two additional, very broad bands appear at 2106 and 2119 cm^{-1} (Figure 3b), indicating additional heterogeneity. The increase of these bands with decreasing pH suggests that they are associated with the A_0 conformation. Protonation and concomitant relocation of the H64 imidazole side chain towards the solvent and the

missing salt bridge result in a solvent-accessible distal pocket. The presence of solvent molecules will broaden and shift the photoproduct bands. In H64L NgbCO and H64L/K67L NgbCO, we observe essentially a single photoproduct band B at 2126 cm^{-1}, quite similar to H64L MbCO, where only one photoproduct band for site B is resolved [52]. The distinct change in frequency indicates that electrostatic interactions between H64 and CO are a major determinant also for the CO stretching frequency in the photoproduct, as recently proposed for MbCO [52]. More importantly, the observed change with this mutation allows a prediction about the actual location of site B. Most likely, the site is very similar to the one in MbCO, on top of and parallel to the heme plane. We also note that the presence of a single CO band in the absence of H64 arises from a lack of Stark splitting, and the ligands are still likely to reside in two orientations in the primary docking site B.

Upon cooling the NgbCO samples from 140 to 3 K under steady illumination, photolyzed CO molecules give rise to a new, prominent band C at 2134 cm^{-1} (Figure 3a). We assign this feature to the secondary docking site that we have already alluded to earlier to interpret the kinetic traces in Figure 2. As all photoproduct bands associated with site C have an identical frequency, site C cannot be located in the immediate vicinity of the active site; otherwise, point mutations (especially the replacement of the H64) should affect its frequency.

3.4. Intermediate Ligand Docking Sites and Recombination

To study CO migration between and recombination from intermediate sites B and C in Ngb, we performed TDS measurements after 1-s illumination at 3 K. All contour plots displaying absorbance changes in the A substate bands of heme-bound CO (Figure 4, left) show strong rebinding features already at 3 K, implying very low activation barriers for geminate rebinding from site B (Figure 4a). The $g(H_{BA})$ distribution calculated from fitting the TDS data (absorbance integrated over all wavenumbers) of wt NgbCO (Figure 4a) peaks at 1.1 kJ/mol (Figure 2, inset), as does the Γ-distribution that fitted the kinetic traces in Figure 2. However, the TDS distribution is much broader, suggesting that processes must have occurred during the course of the TDS temperature ramp that produced an increased fraction of higher barriers. A possible scenario is thermally activated ligand migration from the initial docking site B toward the secondary docking site C. Indeed, positive contours at $\sim$20 K in the photoproduct map (Figure 4b) indicate ligand migration from site B to site C at this temperature. Ligand migration is (to different extents) apparent in all photoproduct maps and thus common to all four samples studied. After slow cooling of the samples under illumination from 140 to 3 K, ligand rebinding occurs on average at higher temperatures, as shown for the wt NgbCO sample in Figures 5a, b. In Figures 5c, d, we have calculated the difference between the two maps in Figures 4a, b and 5a, b. From these maps, it is evident that recombination proceeds predominantly from state C after slow-cool illumination. Dotted (solid) contours in Figure 5c indicate less (more) recombination at lower (higher) temperatures after extended

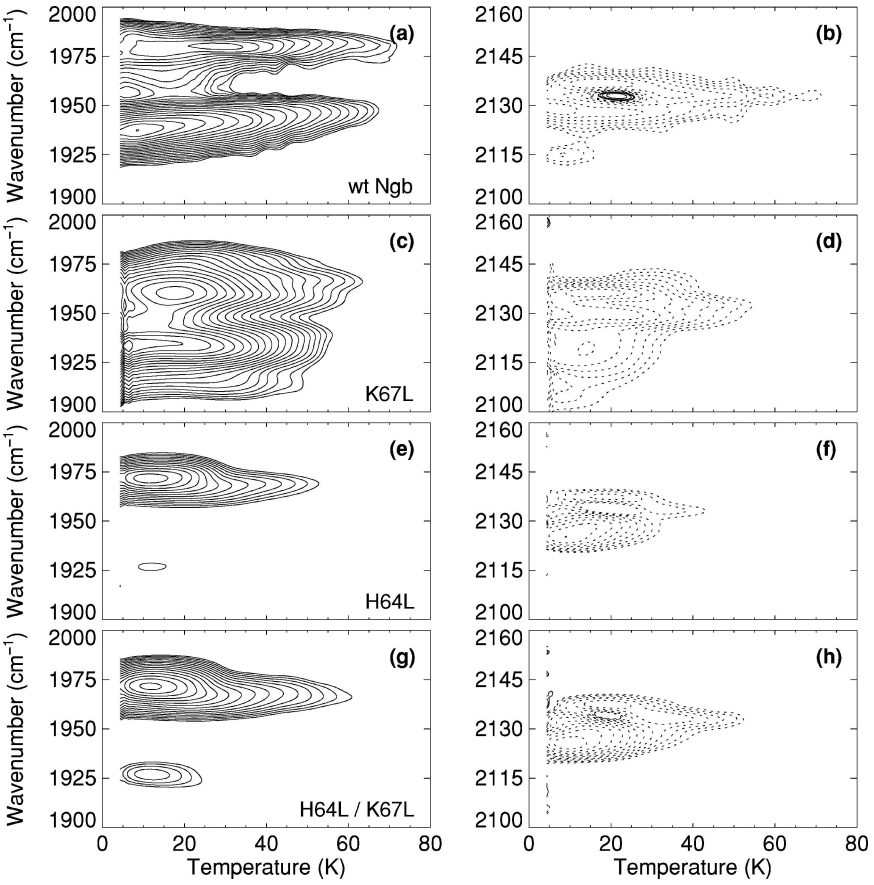

Figure 4. TDS contour maps of wt NgbCO and mutants K67L, H64L and H64L-K67L (1-s illumination at 3 K). Absorbance changes are shown for the IR bands of heme-bound CO (left column) and photolyzed CO (right column). Contours are spaced logarithmically, solid (dotted) lines represent increasing (decreasing) absorbance.

illumination. Dotted contours in Figure 5d represent an increased loss of the C state band upon extended illumination and thus increased recombination from this state.

In NgbCO, the temperature for recombination from the secondary site (30–60 K) is still rather low. In MbCO, rebinding from the primary docking site B peaks at ∼48 K, which corresponds to a barrier of 10 kJ/mol [25, 52]. After extended illumination, ligands are trapped in two internal cavities, Xe4 (Figure 1, site C) and Xe1 (Figure 1, site D), from where they rebind at markedly increased temperatures, ∼80 and ∼125 K [19]. These data indicate that the barriers along the migration pathways between sites B and C in NgbCO are rather low, which suggests that both B and C docking sites are both within the huge internal cavity of Ngb [32, 35]. In Mb, however, the secondary docking sites are separate cavities, and higher barriers have to be overcome for recombination from C and D.

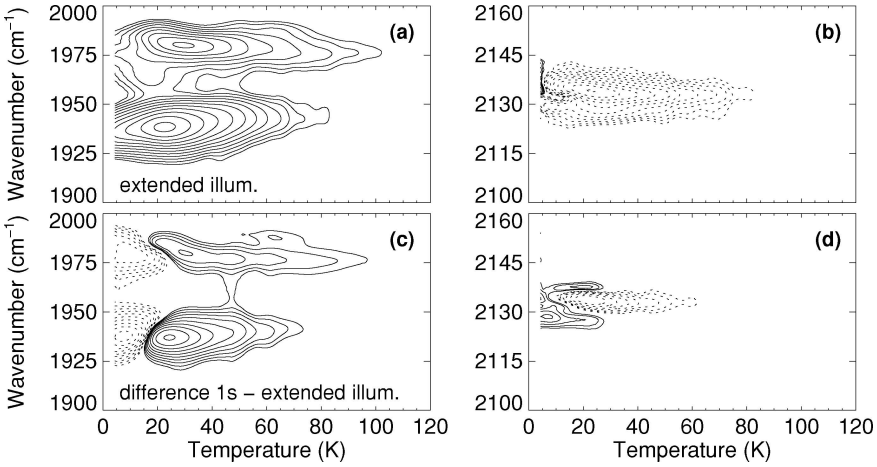

Figure 5. (a, b) TDS contour maps of wt NgbCO after slow cooling under illumination from 140 to 3 K. Absorbance changes are shown for the IR bands of heme-bound CO (left column) and photolyzed CO (right column). Contours are spaced logarithmically, solid (dotted) lines represent increasing (decreasing) absorbance. (c, d) Difference maps between NgbCO TDS contour plots after 1-s (Figures 4a, b) and extended illumination (Figures 5a, b).

4. Conclusions

Using FTIR spectroscopy in the CO stretching bands and flash photolysis with monitoring in the visible range, we have investigated structural heterogeneity in Ngb and its effects on CO binding and migration. A small number of CO stretching bands were identified; they correspond to taxonomic substates that differ in their detailed structure and ligand binding properties. By comparison of bound-state and photoproduct IR spectra of the wt protein with distal pocket mutants and Mb, we were able to provide structural interpretations of the conformations associated with the different CO bands. Moreover, we investigated ligand migration to the primary docking site B. Rebinding from this site is governed by very low enthalpy barriers ($\sim$1 kJ/mol) due to a highly reactive heme iron. We also observed ligand migration to a secondary docking site C, from which CO binding involves somewhat higher barriers. In view of the ongoing, detailed investigations of the structure, dynamics and function of Ngb, we anticipate that the physiological function of Ngb will be elucidated in the near future.

Acknowledgments

This work was supported by grants from the Deutsche Forschungsgemeinschaft (Ni291/3) and the Fonds der Chemischen Industrie. We thank Drs. T. Burmester and T. Hankeln (University of Mainz, Germany) for kindly providing the murine Ngb expression system, Uwe Theilen for constructing and producing the neuroglobin mutants used in this study, and Pengchi Deng for technical assistance.

References

1. Stryer, L.: *Biochemistry*, 4th ed., Freeman, San Francisco, 1995.
2. Nienhaus, G.U. and Young, R.D.: *Protein dynamics*, VCH, New York, 1996.
3. Frauenfelder, H., Sligar, S.G. and Wolynes, P.G.: The Energy Landscapes and Motions of Proteins, *Science* **254** (1991), 1598–1603.
4. Ansari, A., Berendzen, J., Bowne, S.F., Frauenfelder, H., Iben, I.E., Sauke, T.B., Shyamsunder, E. and Young, R.D.: Protein States and Proteinquakes, *Proc. Natl. Acad. Sci. U.S.A.* **82** (1985), 5000–5004.
5. Ansari, A., Berendzen, J., Braunstein, D., Cowen, B.R., Frauenfelder, H., Hong, M.K., Iben, I.E., Johnson, J.B., Ormos, P., Sauke, T.B., *et al*.: Rebinding and Relaxation in the Myoglobin Pocket, *Biophys. Chem.* **26** (1987), 337–355.
6. Andrews, B.K., Romo, T., Clarage, J.B., Pettitt, B.M. and Phillips, G.N., Jr.: Characterizing Global Substates of Myoglobin, *Structure* **6** (1998), 587–594.
7. Garcia, A.E., Blumenfeld, R., Hummer, G. and Krumhansl, J.A.: Multi-Basin Dynamics of a Protein in a Crystal Environment, *Physica D* **107** (1997), 225–239.
8. Becker, O.M. and Karplus, M.: The Topology of Multidimensional Potential Energy Surfaces: Theory and Application to Peptide Structure and Kinetics, *J. Chem. Phys.* **106** (1997), 1495–1517.
9. McMahon, B.H., Müller, J.D., Wraight, C.A. and Nienhaus, G.U.: Electron Transfer and Protein Dynamics in the Photosynthetic Reaction Center, *Biophys. J.* **74** (1998), 2567–2587.
10. Thorn, L.D. and Wiersma, D.A.: Real Time Observation of Low-Temperature Protein Motions, *Phys. Rev. Lett.* **74** (1995), 2138–2141.
11. Hofmann, C., Aartsma, T.J., Michel, H. and Kohler, J.: Direct Observation of Tiers in the Energy Landscape of a Chromoprotein: A Single-Molecule Study, *Proc. Natl. Acad. Sci. U.S.A.* **100** (2003), 15534–15538.
12. Braunstein, D.P., Chu, K., Egeberg, K.D., Frauenfelder, H., Mourant, J.R., Nienhaus, G.U., Ormos, P., Sligar, S.G., Springer, B.A. and Young, R.D.: Ligand Binding to Heme Proteins: III. FTIR Studies of His-E7 and Val-E11 Mutants of Carbonmonoxymyoglobin, *Biophys. J.* **65** (1993), 2447–2454.
13. Li, T., Quillin, M.L., Phillips, G.N., Jr. and Olson, J.S.: Structural Determinants of the Stretching Frequency of CO Bound to Myoglobin, *Biochemistry* **33** (1994), 1433–1446.
14. Vojtechovsky, J., Chu, K., Berendzen, J., Sweet, R.M. and Schlichting, I.: Crystal Structures of Myoglobin-Ligand Complexes at Near-Atomic Resolution, *Biophys. J.* **77** (1999), 2153–2174.
15. Johnson, J.B., Lamb, D.C., Frauenfelder, H., Müller, J.D., McMahon, B., Nienhaus, G.U. and Young, R.D.: Ligand Binding to Heme Proteins. VI. Interconversion of Taxonomic Substates in Carbonmonoxymyoglobin, *Biophys. J.* **71** (1996), 1563–1573.
16. Müller, J.D., McMahon, B.H., Chien, E.Y., Sligar, S.G. and Nienhaus, G.U.: Connection between the Taxonomic Substates and Protonation of Histidines 64 and 97 in Carbonmonoxy Myoglobin, *Biophys. J.* **77** (1999), 1036–1051.
17. Kriegl, J.M., Nienhaus, K., Deng, P., Fuchs, J. and Nienhaus, G.U.: Ligand Dynamics in a Protein Internal Cavity, *Proc. Natl. Acad. Sci. U.S.A.* **100** (2003), 7069–7074.
18. Alben, J.O., Beece, D., Bowne, S.F., Doster, W., Eisenstein, L., Frauenfelder, H., Good, D., McDonald, J.D., Marden, M.C., Moh, P.P., Reinisch, L., Reynolds, A.H., Shyamsunder, E. and Yue, K.T.: Infrared Spectroscopy of Photodissociated Carboxymyoglobin at Low Temperatures, *Proc. Natl. Acad. Sci. U.S.A.* **79** (1982), 3744–3748.
19. Nienhaus, K., Deng, P., Kriegl, J.M. and Nienhaus, G.U.: Structural Dynamics of Myoglobin: The Effect of Internal Cavities on Ligand Migration and Binding, *Biochemistry* **42** (2003), 9647–9658.
20. Nienhaus, K., Deng, P., Kriegl, J.M. and Nienhaus, G.U.: Structural Dynamics of Myoglobin: Spectroscopic and Structural Characterization of Ligand Docking Sites in Myoglobin Mutant L29W, *Biochemistry* **42** (2003), 9633–9646.

21. Nienhaus, K., Deng, P., Olson, J.S., Warren, J.J. and Nienhaus, G.U.: Structural Dynamics of Myoglobin: Ligand Migration and Binding in Valine 68 Mutants, *J. Biol. Chem.* **278** (2003), 42532–42544.
22. Nienhaus, G.U., Mourant, J.R., Chu, K. and Frauenfelder, H.: Ligand Binding to Heme Proteins: The Effect of Light on Ligand Binding in Myoglobin, *Biochemistry* **33** (1994), 13413–13430.
23. Ostermann, A., Waschipky, R., Parak, F.G. and Nienhaus, G.U.: Ligand Binding and Conformational Motions in Myoglobin, *Nature* **404** (2000), 205–208.
24. Lim, M., Jackson, T.A. and Anfinrud, P.A.: Mid-Infrared Vibrational Spectrum of CO after Photodissociation from Heme: Evidence for a Ligand Docking Site in the Heme Pocket of Hemoglobin and Myoglobin, *J. Chem. Phys.* **102** (1995), 4355–4366.
25. Lim, M., Jackson, T.A. and Anfinrud, P.A.: Ultrafast Rotation and Trapping of Carbon Monoxide Dissociated from Myoglobin, *Nat. Struct. Biol.* **4** (1997), 209–214.
26. Tilton, R.F., Jr., Kuntz, I.D., Jr. and Petsko, G.A.: Cavities in proteins: Structure of a Metmyoglobin-Xenon Complex Solved to 1.9 Å, *Biochemistry* **23** (1984), 2849–2857.
27. Burmester, T., Weich, B., Reinhardt, S. and Hankeln, T.: A Vertebrate Globin Expressed in the Brain, *Nature* **407** (2000), 520–523.
28. Venis, S.: Neuroglobin might Protect Brain Cells During Stroke, *Lancet* **358** (2001), 2055.
29. Sun, Y., Jin, K., Mao, X.O., Zhu, Y. and Greenberg, D.A.: Neuroglobin is Up-Regulated by and Protects Neurons from Hypoxic-Ischemic Injury, *Proc. Natl. Acad. Sci. U.S.A.* **98** (2001), 15306–15311.
30. Sun, Y., Jin, K., Peel, A., Mao, X.O., Xie, L. and Greenberg, D.A.: Neuroglobin Protects the Brain from Experimental Stroke in vivo, *Proc. Natl. Acad. Sci. U.S.A.* **100** (2003), 3497–3500.
31. Wakasugi, K., Nakano, T. and Morishima, I.: Oxidized Human Neuroglobin Acts as a Heterotrimeric Galpha Protein Guanine Nucleotide Dissociation Inhibitor, *J. Biol. Chem.* **278** (2003), 36505–36512.
32. Vallone, B., Nienhaus, K., Matthes, A., Brunori, M. and Nienhaus, G.U.: The Structure of Carbonmonoxy Neuroglobin Reveals a Heme-Sliding Mechanism for Control of Ligand Affinity, *Proc. Natl. Acad. Sci. U.S.A.*, in press.
33. Kriegl, J.M., Bhattacharyya, A.J., Nienhaus, K., Deng, P., Minkow, O. and Nienhaus, G.U.: Ligand Binding and Protein Dynamics in Neuroglobin, *Proc. Natl. Acad. Sci. U.S.A.* **99** (2002), 7992–7997.
34. Pesce, A., Dewilde, S., Nardini, M., Moens, L., Ascenzi, P., Hankeln, T., Burmester, T. and Bolognesi, M.: Human Brain Neuroglobin Structure Reveals a Distinct Mode of Controlling Oxygen Affinity, *Structure (Camb.)* **11** (2003), 1087–1095.
35. Vallone, B., Nienhaus, K., Brunori, M. and Nienhaus, G.U.: The Structure of Murine Neuroglobin: Novel Pathways for Ligand Migration and Binding, *Proteins* **56** (2004), 85–92.
36. Nienhaus, K., Kriegl, J.M. and Nienhaus, G.U.: Structural Dynamics in the Active Site of Murine Neuroglobin and Its Effects on Ligand Binding, *J. Biol. Chem.* **279** (2004), 22944–22952.
37. Dewilde, S., Kiger, L., Burmester, T., Hankeln, T., Baudin-Creuza, V., Aerts, T., Marden, M.C., Caubergs, R. and Moens, L.: Biochemical Characterization and Ligand Binding Properties of Neuroglobin, a Novel Member of the Globin Family, *J. Biol. Chem.* **276** (2001), 38949–38955.
38. Trent, J.T., Watts, R.A. and Hargrove, M.S.: Human Neuroglobin, a Hexacoordinate Hemoglobin that Reversibly Binds Oxygen, *J. Biol. Chem.* **276** (2001), 30106–30110.
39. Uno, T., Ryu, D., Tsutsumi, H., Tomisugi, Y., Ishikawa, Y., Wilkinson, A.J., Sato, H. and Hayashi, T.: Residues in the Distal Heme Pocket of Neuroglobin: Implications for the Multiple Ligand Binding Steps, *J. Biol. Chem.* **279** (2003), 5886–5893.
40. Lamb, D.C., Nienhaus, K., Arcovito, A., Draghi, F., Miele, A.E., Brunori, M. and Nienhaus, G.U.: Structural Dynamics of Myoglobin: Ligand Migration Among Protein Cavities Studied by Fourier Transform Infrared/Temperature Derivative Spectroscopy, *J. Biol. Chem.* **277** (2002), 11636–11644.

41. Nienhaus, G.U. and Nienhaus, K.: Infrared Study of Carbon Monoxide Migration among Internal Cavities of Myoglobin Mutant L29W, *J. Biol. Phys.* **28** (2002), 163–172.
42. Berendzen, J. and Braunstein, D.: Temperature-Derivative Spectroscopy: A Tool for Protein Dynamics, *Proc. Natl. Acad. Sci. U.S.A.* **87** (1990), 1–5.
43. Mourant, J.R., Braunstein, D.P., Chu, K., Frauenfelder, H., Nienhaus, G.U., Ormos, P. and Young, R.D.: Ligand Binding to Heme Proteins: II. Transitions in the Heme Pocket of Myoglobin, *Biophys. J.* **65** (1993), 1496–1507.
44. Young, R.D. and Bowne, S.F.: Conformational Substates and Barrier Height Distributions in Ligand Binding to Heme Proteins, *J. Chem. Phys.* **81** (1984), 3730–3737.
45. Lamb, D.C., Kriegl, J., Kastens, K. and Nienhaus, G.U.: Quantum-Mechanical Tunneling of Water in Heme Proteins, *J. Phys. Org. Chem.* **13** (2000), 1–5.
46. Alben, J.O., Beece, D., Bowne, S.F., Eisenstein, L., Frauenfelder, H., Good, D., Marden, M., Moh, P.P., Reinisch, L., Reynolds, A.H. and Yue, K.T.: Isotope Effect in Molecular Tunneling, *Phys. Rev. Lett.* **44** (1980), 1157–1160.
47. Steinbach, P.J., Chu, K., Frauenfelder, H., Johnson, J.B., Lamb, D.C., Nienhaus, G.U., Sauke, T.B. and Young, R.D.: Determination of Rate Distributions from Kinetic Experiments, *Biophys. J.* **61** (1992), 235–245.
48. Steinbach, P.J., Ansari, A., Berendzen, J., Braunstein, D., Chu, K., Cowen, B.R., Ehrenstein, D., Frauenfelder, H., Johnson, J.B., Lamb, D.C., Luck, S., Mourant, J.R., Nienhaus, G.U., Ormos, P., Philipp, R., Xie, A. and Young, R.D.: Ligand Binding to Heme Proteins: Connection Between Dynamics and Function, *Biochemistry* **30** (1991), 3988–4001.
49. Austin, R.H., Beeson, K.W., Eisenstein, L., Frauenfelder, H. and Gunsalus, I.C.: Dynamics of Ligand Binding to Myoglobin, *Biochemistry* **14** (1975), 5355–5373.
50. Ormos, P., Szaraz, S., Cupane, A. and Nienhaus, G.U.: Structural Factors Controlling Ligand Binding to Myoglobin: A Kinetic Hole-Burning Study, *Proc. Natl. Acad. Sci. U.S.A.* **95** (1998), 6762–6767.
51. Phillips, G.N., Jr., Teodoro, M.L., Li, T., Smith, B. and Olson, J.S.: Bound CO is a Molecular Probe of Electrostatic Potential in the Distal Pocket of Myoglobin, *J. Phys. Chem. B* **103** (1999), 8817–8829.
52. Nienhaus, K., Olson, J.S., Franzen, S. and Nienhaus, G.U.: The Origin of Stark Splitting in the Initial Photoproduct State of MbCO, *J. Am. Chem. Soc.* **127** (2005), 40–41.
53. Yang, F. and Phillips, G.N., Jr.: Crystal Structures of CO-, Deoxy- and Met-Myoglobins at Various pH Values, *J. Mol. Biol.* **256** (1996), 762–774.
54. Alben, J.O. and Caughey, W.S.: An Infrared Study of Bound Carbon Monoxide in the Human Red Blood Cell, Isolated Hemoglobin, and Heme Carbonyls, *Biochemistry* **7** (1968), 175–183.
55. Ray, G.B., Li, X.-Y., Ibers, J.A., Sessler, J.L. and Spiro, G.S.: How Far can Proteins Bend the FeCO Unit, *J. Am. Chem. Soc.* **116** (1994), 162–176.
56. Couture, M., Burmester, T., Hankeln, T. and Rousseau, D.L.: The Heme Environment of Mouse Neuroglobin. Evidence for the Presence of two Conformations of the Heme Pocket, *J. Biol. Chem.* **276** (2001), 36377–36382.
57. Bhattacharya, S., Sukits, S.F., MacLaughlin, K.L. and Lecomte, J.T.: The Tautomeric State of Histidines in Myoglobin, *Biophys. J.* **73** (1997), 3230–3240.
58. Yeh, S.R., Couture, M., Ouellet, Y., Guertin, M. and Rousseau, D.L.: A Cooperative Oxygen Binding Hemoglobin from Mycobacterium Tuberculosis. Stabilization of Heme Ligands by a Distal Tyrosine Residue, *J. Biol. Chem.* **275** (2000), 1679–1684.
59. Schlichting, I., Berendzen, J., Phillips, G.N., Jr. and Sweet, R.M.: Crystal Structure of Photolysed Carbonmonoxy-Myoglobin, *Nature* **371** (1994), 808–812.